



## Numerical Modelling for Incompressible Flows

# Assignment

Marc Barcelo  
January 2020

MSc Aerospace Computational Engineering

# Index

---

Abstract.....	4
Introduction.....	4
Theory Fundamentals .....	5
Problem characteristics .....	10
Results .....	13
· Coarse Mesh Study.....	15
· Upwind Scheme.....	16
· Central Scheme.....	19
· Fine Mesh Study .....	21
Conclusions .....	25
References .....	26
Appendix 1: Medium Mesh Study .....	27

## List of Figures

Figure 1. Staggered Grid Scheme .....	6
Figure 2. Lid-driven cavity problem.....	10
Figure 3. Mesh Boundary Conditions for the Staggered Distribution .....	11
Figure 4. Parameters for "Ghia et al" operation conditions.....	13
Figure 5. Cavity Schemes: Data Axis .....	14
Figure 6. Comparison between reference data and computed data: velocity components.....	14
Figure 7. Coarse Mesh. U and V comparison for Upwind and Central schemes.....	16
Figure 8. U and V components surface inside the cavity. Upwind scheme, Coarse Mesh.....	17
Figure 9. Streamlines of Cavity's velocity field. Upwind scheme, Coarse mesh.....	18
Figure 10. Velocity field vectors.....	19
Figure 11 Streamlines of Cavity's velocity field. Central scheme, Coarse mesh .....	20
Figure 12. U and V components surface inside the cavity. Central scheme, Coarse Mesh.....	20
Figure 13. Fine Mesh. U and V comparison for Upwind and Central schemes.....	21
Figure 14. U and V components surface inside the cavity for both schemes (above: Upwind, below: Central). Fine Mesh .....	22
Figure 15. Streamlines of the velocity field for both schemes (above: Upwind, below: Central). Fine Mesh .....	23
Figure 16. Vorticity Magnitude along the flow inside the cavity, Central Scheme, Fine Mesh...	24

Figure 17. Medium Mesh Velocity comparison for both schemes in the geometrical medium profile .....	27
Figure 18. Medium Mesh. Streamlines for: Upwind Scheme (left) and Central Scheme (right) ..	28
Figure 19. Medium Mesh. Pressure distribution: Upwind scheme (left) and Central Scheme (right) ..	29

## List of Equations

Equation 1. Incompressible Flow Continuity Equation.....	5
Equation 2. Incompressible Flow Momentum Equation.....	5
Equation 3. Pressure Components - Intermediate + Correction.....	7
Equation 4. Pressure Correction Equation with under-relaxation factor.....	7
Equation 5. Pressure-Poisson Equation.....	7
Equation 6. Flux Conservation.....	7
Equation 7. Flux Conservation Decomposition.....	7
Equation 8. Pressure Correction Equation in Implicit Centered Form.....	8

## List of Tables

Table 1. Norms Upwind - Central Difference Scheme. Re=400, Grid 129x129 points.....	15
Table 2. Norms Upwind - Central Difference Scheme. Re=65, Grid 10x10 points .....	16
Table 3. Norms Upwind - Central Difference Scheme. Re=65, Grid 250x250 points.....	21
Table 4. Medium Mesh Deviations from both schemes for the velocity components.....	27
Table 5. Medium Mesh. Norms for the Pressure Deviation for both schemes .....	29

## List of Symbols

Re: Reynolds number	$\bar{u}$ : velocity field
N-S: Navier-Stokes	$U$ : x-axis component of velocity
TDMA: Tridiagonal Matrix Algorithm	$V$ : y-axis component of velocity
SIMPLE: Semi-Implicit Method for Pressure	$\nu$ : kinematic viscosity
Linked Equations	$\nabla$ : gradient operator
$\rho$ : Density	$\nabla^2$ : Laplacian operator
$p$ : pressure	$\nabla \otimes$ : dyadic product
$g$ : gravity	$\omega$ : under relaxation parameter

## **Abstract**

The aim of this document is to evaluate the performance of the Incompressible Flow Numerical Model of Pressure Correction developed by (Patankar and Spalding, 1972) to simulate the bidimensional flow ( $Re=65$ ) over the benchmark problem lid driven cavity ( $1m \times 1m$ ). Here, the main program code in FORTRAN language is given for a channel problem; hence the boundary conditions for the cavity geometry will be implemented, and the upwind and central difference schemes for the convective term will be computed and compared. The code, however, will also be validated with the same scenario and case explained in (Ghia, Ghia and Shin, 1982)

Results of the simulation will be computed using MATLAB and ParaView software and will suggest the convenience of performing a further refinement of the coarse grid. This refinement, as it will be seen, will depend on the Reynolds number of the flow but also in the accuracy order of the scheme. Besides, a further explanation on the SIMPLE algorithm, TDMA solver and Staggered Grid geometry will be provided.

## **Introduction**

Flow nature can be described depending on the value of its parameters. Fluid magnitudes have a huge impact on each other as governing equations demonstrate. Quite all of them - somehow- are related in the end. From them, we can explain the - initially hard to understand - example of how diffusor and nozzle geometries switch their behavior depending on the velocity of the flow. But pressure is at the same time related to the velocity through the momentum equation, then a gradient of pressures between two points will induce a movement of flow (velocity) between these points as seen in the Poiseuille problem (see (Landau L.D. and Lifshitz E.M., 1987)), and releasing at the same time a variation of most of the other extensive magnitudes.

Thus, to easily and rapidly clarify which kind of flow behavior is faced, science classifies flow natures. Depending on if the velocity magnitude in a particular axis is higher than local sound speed, flow will be distinguished into subsonic, transonic or supersonic. Each case will describe different flow behavior and will be therefore approached through different numerical schemes. In a similar manner, flow can be equally differentiated if it is compressible or incompressible. Here, this last case will be treated and detailed.

An incompressible flow is characterized by operating under  $M<0.3$ , to have quasi-constant density along the flow and specially the fact that the divergence of the velocity field is 0, what is known as the incompressibility constraint. The pressure is no longer a function of density and vice versa, as the equation of state is not satisfied under these premises. A wide variety of numerical solvers have been developed to withdraw solutions to the Navier-Stokes equations under different assumptions or points of view. This scenario is specially interesting to industry, since most of liquids can be considered to be incompressible. Hence, here the “industrial” Pressure-Correction Model developed by (Patankar and Spalding, 1972) will be analyzed and applied to the Cavity Problem.

## Theory Fundamentals

### · Governing Equations

The Equations that will describe the nature and fluid magnitudes of incompressible flows can be derived from the general Navier-Stokes Equation (compressible case) by imposing the incompressible flow constraints ( $\rho = ct$ ,  $M \leq 0.2$ ,  $\nabla \cdot \bar{u} = 0$ ). Then, the three conservation formulas to be used will result in:

#### · Continuity Equation

$$\nabla \cdot \bar{u} = 0 \quad (1)$$

#### · Navier-Stokes Momentum Equation

$$\frac{\partial \bar{u}}{\partial t} + \bar{u} \cdot (\nabla \otimes \bar{u}) = \bar{g} - \frac{1}{\rho} \cdot \nabla p + \nu \cdot \nabla^2 \bar{u} \quad (2)$$

As it has been already pointed out, the thermodynamic state equation cannot be used since pressure is not a function of density and vice versa. Then, the missing equation to be able to solve the undetermined and non-linear system of equations will depend on the incompressible numerical model applied. Some attempts to achieve analytical solutions such as the Burger's equation have been done, however their applicability is under really restrictive conditions. Thus, computational methods remain the first choice in most of cases. Usually it will involve solving parabolic or hyperbolic partial derivative system of equations and most of times lead to the Poisson equation. However, in the Pressure Correction model, the SIMPLE algorithm will be used and explained in the following pages.

### · Staggered Grid – Finite Volume

The Finite Element Method is widely applied in numerical schemes to solve the continuous problem with a discrete grid -nodal structure- without losing essential generality in the process. The nature of the unknown is set to a concrete region -or node- and then conducted to the whole structure through the assembly equations, describing accurately the physical and continuous problem. For this document, so as to use the SIMPLE Algorithm, the Staggered Grid geometry will be performed.

With the term “staggered” -contrary to “collocated”- it is seen that the set of variables will not be applied in the same point of each node. This is specially beneficial when separate unknown functions are solved at the same time.

Serve the following image as a representative cell i,j (will be referred with the “p”) with its adjacent cells – North, West, South and East. The propagation and variation of the fluid magnitudes will be transmitted through their interaction, given by the coefficients of the discretized differential equation to be solved. The pressure values will be set in the center of the cells whils velocity components will be placed in the cell faces as Figure 1shows.

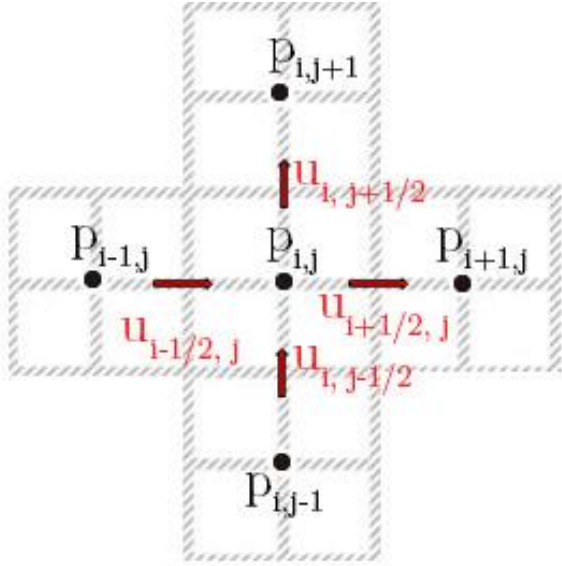


Figure 1. Staggered Grid Scheme

The dependence on the neighboring values -in i and j direction- will lead to a tridiagonal matrix multiplying the unknown term for each space direction once the implicit equation is obtained.

- SIMPLE Algorithm

Deriving its name from Semi-Implicit Method for Pressure Linked Equations, it describes a procedure based on iteration of a particular numerical discretization for the Incompressible Flow Conservative Governing Equations.

It was primarily conceived by (Patankar and Spalding, 1972) as an “engineering-type” method to give efficient, practical but accurate solutions in contrast with the Boundary-Layer Theory implementation predominant in most of academical numerical procedures for Incompressible Flows. Although these last ones are the most interesting for academia, industry prioritizes in the less complex and consuming procedures for obvious reasons. Thus, added to the fact that the flow is treated as a parabolic 2-D flow with pressure corrections instead of facing the real 3-D elliptic equations made this method outstand in the industry environment.

The main idea of the procedure is to start from a “known” or “estimate” pressure in the boundary layers, then use them to calculate the intermediate velocity field by satisfying the Momentum Navier-Stokes equations in all the dimensions of the problem. The more precise this guess is, the faster converged results will be obtained. Subsequently, this velocity field will not satisfy -at the same time- the Incompressible Continuity equation. This is why it will be called intermediate velocity field: it only supposes a further step until both pressure and velocity fields are accurate enough – predefined by a convergence parameter or number of maximum iterations that will be beforehand fixed - to satisfy the flow restrictions (equations).

Thus, an iterative correction in the intermediate velocity field yet mainly to the pressure field must be done by adding a pressure correction term ( $p'$ ) as it follows in the equation:

$$p = p^* + p' \quad (3)$$

Being  $p'$  an additional term to be computed that makes both pressure and later velocity fields satisfy the continuity equation.

However, experience from numerical solutions obtained by this method may suggest that the addition of the term  $p'$  may derive error divergence, mainly caused by non-linearity of the solution. Then, an underrelaxation parameter  $\omega$  -taking values between 0 and 1- is normally applied to expedite solution convergence. According to this, the previous equation can be better corrected to:

$$p = p^* + \omega \cdot p' \quad (4)$$

The calculation of  $p'$  is directly related to the residual mass flow. If flux is unsteady, the Poisson equation used in other incompressible flow methods:

$$\nabla^2 p = \frac{\rho}{\Delta t} \cdot (\nabla \cdot \bar{u}) \quad (5)$$

must be computed. Note the case to be solved within this document represents the steady flow over a cavity. Hence, using the Finite-Volume treatment, an equation will be derived from mass flux (continuity) calculus.

Note, from U and V Momentum equations, that u and v components of velocities depend on the immediate surrounding (let's say, neighbor) cell values of velocity but also from their values of: mainly pressure gradient, and other minor contributions due to viscosity, gravity, and additional terms that will be neglected in here.

As a first and rapid approximation, when applying the flux correction from continuity, these neighboring values will not be also considered due to the predominant effect introduced by the pressure gradient. Thus, we will obtain the needed equation relating velocity correction with pressure correction. Using the Finite-Element notation,

$$\begin{aligned} a_e \cdot u'_e &\approx \Delta y \cdot (p'_p - p'_E) \\ a_N \cdot v'_n &\approx \Delta y \cdot (p'_p - p'_N) \end{aligned}$$

By attending in the pressure centroid of each finite volume, the flux conservation must be satisfied, then, using the staggered cell notation in the normal sign convention:

$$F_N - F_S + F_E - F_W = 0 \quad (6)$$

So far, the only variable known are both pressure and velocity fields obtained by an initial guess of pressure and isolation of velocity from U and V Momentum equations -intermediate velocity field noted with \*- then, as said, continuity is not satisfied. This is where we will impose our continuity criteria along with pressure's relationship with velocity.

$$F_N^* - F_S^* + F_E^* - F_W^* \neq 0$$

but, if it is corrected with additional correction terms:

$$F_N^* + F'_N - (F_S^* + F'_S) + (F_E^* + F'_E) - (F_W^* + F'_W) = 0 \quad (7)$$

The  $F_{\_}^*$  terms are known from the intermediate velocity and pressure field thence the correction terms can be calculated. Therefore, computing the fluxes of the correction terms and isolating the pressure in the i,j cell center (point p)

$$F_N^* + \rho \cdot d_N \cdot \Delta y \cdot (p'_p - p'_E) + -(F_S^* + \rho \cdot d_S \cdot \Delta x \cdot (p'_S - p_p)) + (F_E^* + \rho \cdot d_E \cdot \Delta y \cdot (p'_p - p'_E)) - (F_W^* + \rho \cdot d_W \cdot \Delta y \cdot (p'_W - p'_p)) = 0$$

The final pressure correction equation -grouping terms into parameters- will look like the following:

$$a_p \cdot p'_p = \sum_{nb} a_{nb} \cdot p'_{nb} + b \quad (8)$$

being:

- sub index nb: neighboring values (north, west, south, east)
- $a_p = \sum_{nb} a_{nb}$
- no-satisfaction of the continuity term  $b = F_N^* - F_S^* + F_E^* - F_W^*$

Once obtained the pressure correction term using the Implicit Solver TDMA due to the tridiagonal matrix form caused by the neighboring values in each dimension (terms i-1, i, i+1 and j-1, j, j+1), the velocity is corrected and again is introduced to the Momentum Equation and running this iteration until the solution converges for each fluid magnitude converges or the maximum number of iterations is reached.

Additional equations -such as energy, turbulence, and other transport equations- can be added resulting in an increase of the loop and the computational cost too, since a new matrix is calculated for each and one dimension per equation is introduced in the program.

As it has been remarked, pressure correction  $p'$  is prone to be overestimated and may cause errors diverge, then it is corrected with an under-relaxation parameter  $\omega$  with values proximate to 0.6-0.7. For this simulation, the values of the under-relaxation parameter for  $u'$ ,  $v'$  and  $p'$  magnitudes will be 0.6.

#### • TDMA Procedure

This Gaussian-Elimination Algorithm has already been used in Assignment 1 due to its high great performance at solving tridiagonal matrixes and especially the efficient memory treatment by using vectors instead of matrixes as a result of the sparsity. The choice of the implicit method solver was free yet after reading (Golub and van Loan, 1983) the TDMA Algorithm outstood for solving the One-Dimensional Fourier Equation with Crank-Nicholson and Laasonen schemes.

In this case, the each-dimension dependence of values of previous, current and next cell - or particularly cell faces in the case of velocity- logically lead to a tridiagonal matrix for each dimension which can be efficiently and quickly solved by this algorithm.

Therefore, the TriDiagonal Matrix Algorithm (also known in literature as Thomas Algorithm) solves an implicit formulation of a system of linear equations by – vastly summarized- applying a transformation of matrixes diagonals and to the independent vector in order to get a two diagonal system and then solving the system by equations by applying a forward difference

from the first to the last term followed by a backward difference until reaching again the first term and subsequently solving the unknown variable for each point of the dimension.

Hence, this procedure must be applied for each dimension (including time) and will result in one additional loop per dimension/variable to be obtained. In our program, it will be applied to  $U(i,j)$ ,  $V(i,j)$  but also  $P$  in the pressure correction.

In more detail, the first transformation indicated will be to divide the matrix's superior diagonal (in vector form) and the independent vector by its main diagonal term for the first row. Once achieved, after applying the following forward pseudo-code operation:

- $superiordiagonal[i] = superiordiagonal[i] / (maindiagonal[i] - superiordiagonal[i - 1]) * inferiordiagonal[i];$
- $independent[i] = (independent[i] - independent[i - 1] * inferiordiagonal[i]) / (maindiagonal[i] - superiordiagonal[i - 1] * inferiordiagonal[i])$

Now, the two-diagonal matrix is obtained and only a backward substitution from the  $N$  term to the first one is left to do. The  $N$  term should look like the following one, solving its magnitude and therefore the first value of the solution:

- $independent[N] = (independent[N] - independent[N - 1] * inferiordiagonal[N]) / (maindiagonal[N] - inferiordiagonal[N] * superiordiagonal[N - 1])$
- $solution[N] = independent[N]$

The backward procedure to proceed to achieve the results is the following, and it must go from  $N-1$  to the first term (0 or 1 depending on the programming language)

- $solution[i] = independent[i] - superiordiagonal[i] * solution[i + 1];$

This process must be repeated for each dimension and variable to be solved. The FORTRAN code for the program uses beta and gamma parameters to represent the first transformation explained, the “rhs” (right hand side) to refer to the independent vector and the solution depends in two dimensions instead of one, which basically affects in adding an outer loop. However, it is believed that this short one-dimensional and general explanation in pseudocode of the procedures is more appropriate to understand the Algorithm by itself than directly commenting the code.

## Problem characteristics

The problem to be solved is a lid driven squared cavity ( $L=1$  m,  $D=1$  m), with operation conditions of  $Re=65$ . The program that contains the numerical algorithm is already given, however it is constructed to solve the problem of a bidimensional channel instead of the desired cavity. Then, it is our responsibility to change the boundary conditions within the code to adapt it.

The cavity problem is known to us and conforms one of the most studied basic experiments and cases of Computational Fluid Dynamics. Serve the following image Figure 2 as the physical representation of the problem's geometry.

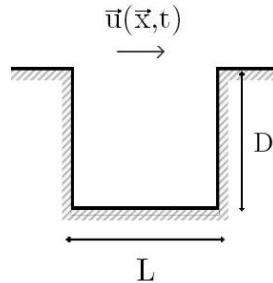


Figure 2. Lid-driven cavity problem

The geometry of the two-dimensional problem shows that three of its four boundary limits consist of impermeable wall (fluid velocity is 0 then its components  $u$  and  $v = 0$ ) but the superior limit obeys the free-stream condition, where flow is predominantly unidirectional in the  $x$  axis ( $u=1$ ,  $v=0$ ). These conditions will be applied in the FORTRAN code, in both subroutines of "U Momentum" and "V Momentum" and using the staggered grid distribution as:

```

· U Momentum
! set boundary conditions for
coefficients in the equations
! south
aw(:,1)=0.
ae(:,1)=0.
as(:,1)=0.
an(:,1)=0.
ap(:,1)=1.
su(:,1)=0.
! west
aw(1,:)=0.
ae(1,:)=0.
as(1,:)=0.
an(1,:)=0.
ap(1,:)=1.

```

$su(1,:)=0.$ $! north$ $aw(:,iNyUNodes)=0.$ $ae(:,iNyUNodes)=0.$ $as(:,iNyUNodes)=0.$ $an(:,iNyUNodes)=0.$ $ap(:,iNyUNodes)=1.$ $su(:,iNyUNodes)=1.$	$! east$ $aw(iNxUNodes,:)=0.$ $ae(iNxUNodes,:)=0.$ $as(iNxUNodes,:)=0.$ $an(iNxUNodes,:)=0.$ $ap(iNxUNodes,:)=1.$ $su(iNxUNodes,:)=0.$
---	--

```

: V Momentum
! south
aw(:,1)=0.
ae(:,1)=0.
as(:,1)=0.
an(:,1)=0.
ap(:,1)=1.
su(:,1)=0.

! west
aw(1,:)=0.
ae(1,:)=0.
as(1,:)=0.
an(1,:)=0.
ap(1,:)=1.
su(1,:)=0.

! north
aw(:,iNyVNodes)=0.
ae(:,iNyVNodes)=0.
as(:,iNyVNodes)=0.
an(:,iNyVNodes)=0.
ap(:,iNyVNodes)=1.
su(:,iNyVNodes)=0.

! east
aw(iNxVNodes,:)=0.
ae(iNxVNodes,:)=0.
as(iNxVNodes,:)=0.
an(iNxVNodes,:)=0.
ap(iNxVNodes,:)=1.
su(iNxVNodes,:)=0.

```

The Pressure correction subroutine must not be changed as it is correctly defined – it does not change from the channel to the cavity case. An example of the resulting grid once applied the boundary conditions could be represented with the following illustrative idea:

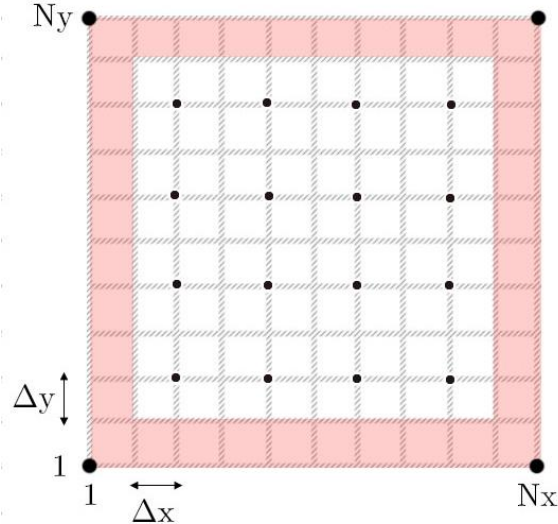


*Figure 3. Mesh Boundary Conditions for the Staggered Distribution*

Now, the solution is set to be solved through the algorithm.

Additionally, we have been asked to implement the central scheme for the convective term as a further step apart from the already implemented upwind scheme. To achieve this, and following (Turquand D'auzay and Asproulis, 2013) for the Momentum Fluxes of U and V, the “a” coefficients and the “su” term must be changed into the following code:

<u>· U Momentum</u>	<u>· V Momentum</u>
$aw(i, j) = dw + gw/2$	$aw(i, j) = dw + gw/2$
$ae(i, j) = - ge/2 + de$	$ae(i, j) = - ge/2 + de$
$as(i, j) = ds + gs/2$	$as(i, j) = ds + gs/2$
$an(i, j) = -gn/2 + dn$	$an(i, j) = -gn/2 + dn$
$ap(i,j)=$	$ap(i,j)=$
$dn+de+dw+ds+0.5*(ge-gw+gn-gs)$	$=dw+de+dn+ds+0.5*(ge-gw+gn-gs)$
$su(i, j) = -(rP(i+1, j) - rP(i, j))*rDY$	$su(i, j) = -(rP(i, j+1) - rP(i,j))*rDX$

According to (Versteeg and Malalasekera, 1995), the choice of using the upwind or the central scheme is sensitive to the Peclet number, that relates advection velocity with diffusion velocity. Hence, it is proven that for the convective term, if  $|Pe| > 2$ , the central difference scheme diverges and the upwind scheme must be applied and that will withdraw decent results. Then, each scheme has its complementary scope of application. Thus, the most sensible action would be to implement an “if” statement and depending on the Peclet number, it will compute the central differencing scheme or the upwind.

However, in the present code, the Peclet number is only applied in the injection subroutine, obtaining the “Scalar” variable, and it is not used at all in the pressure correction algorithm (calculation of u, v and p). Then, both schemes will be equally applied and analyzed in the Results section.

## Results

- Validation of the code

Once proper boundary conditions have been set in the program, the first step to complete is to ensure that results obtained by the FORTRAN program are reliable and accurate. In order to do this, the same scenario from available literature (Ghia, Ghia and Shin, 1982) will be taken and computed in our program and then will be compared to the results from the paper.

The operation conditions from (Ghia, Ghia and Shin, 1982) show a flow over and inside cavity, with dimensions of 1x1 meters, a computational grid (mesh) of 129 x 129 points and flow regime of Re=400. Thus, before compiling the f90 program, our “parameters.par” should look like:

```
1.          ! domain height
1.          ! domain width
400         ! Reynolds
!10.        ! Peclet
!0.         ! Injection start
!0.         ! Injection end
129         ! cells in X
129         ! cells in Y
5000        ! max iterations
1.e-6       ! convergence criteria
0.6         ! P underrelaxation
0.6         ! U underrelaxation
0.6         ! V underrelaxation
!1.         ! Scalar underrelaxation
```

*Figure 4. Parameters for "Ghia et al" operation conditions*

Remember that introducing “!” will be taken as a comment in the “.par” file, then, all the values that are not required will be neglected. The program code, as it has been said, incorporates a subroutine where an injection is simulated, although, this procedure will not be erased from the program as it supposes an interesting case that can be useful in a future.

Once the code is built up and ran by the compiler -in our case, the “ifort” from Linux-data can be extracted and plotted against the incoming from (Ghia, Ghia and Shin, 1982), which will be taken as a reference for accuracy.

According to their authors, the second-order derivatives are treated with second-order accurate central difference scheme, whilst the convective term is modelled with a first-order upwind difference scheme “including its second order accurate term as a deferred correction”. Thus, it can be expected slightly more accuracy from their results than the ones obtained through the FORTRAN code, though they share similarities.

The FORTRAN code uses first order of accuracy upwind difference scheme for the convective term, but also, when implemented, second-order central scheme for the same term. - Its implementation will be discussed in the Central Scheme section.

The results from (Ghia, Ghia and Shin, 1982) represent the values of the U and V components of velocity in geometrical lines - profiles - in the middle of the cavity as the next figure suggests.

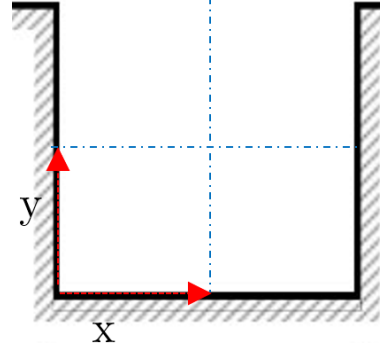


Figure 5. Cavity Schemes: Data Axis

Now, results are plotted and compared in Figure 6

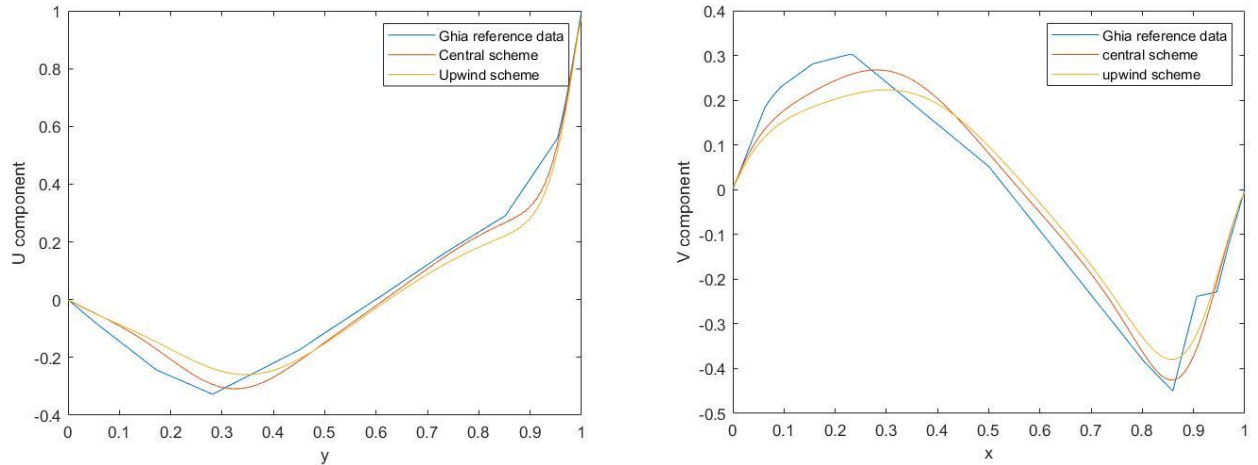


Figure 6. Comparison between reference data and computed data: velocity components.

As it can be perceived in Figure 6, the data provided in(Ghia, Ghia and Shin, 1982) is not enough to describe the curvilinear envelop of both geometries. Only 17 points are available to be graphed while our U and V have, logically, 130 points each. Hence, an abrupt and “too-straight” curve can be noticed and may look like there’s more error than the one that actually is. This is due to the fact that MATLAB and quite most of post-processing programs connects points with straight lines.

However, a huge similarity and accuracy in the three curves can be seen. The highest deviations take place in  $y=0.1705$  for the U component, where there’s a relative error of 40.28% for the upwind and 30.16% for the central scheme in reference to the (Ghia, Ghia and Shin, 1982) data, and in  $x=0.155$  for the V component where it is sighted a 34.42% deviation between upwind and reference curves yet 22% for the central scheme and reference curve as well. Nonetheless, apart from these most conflictive points, all the others seem to demonstrate that the discretization schemes and overall program performs greatly, and hence our program is validated.

Logically, the central scheme will operate with one order of higher accuracy than the upwind scheme does, and then better results can be expected. This hypothesis is reaffirmed with results from Figure 6. The only issue central schemes for first differences can bring is, for linear advection problem, the results turn to be unstable as it can be seen and demonstrated. However, here, due to the influence of the other terms in the N-S equations but also the iterative convergence constraints as well, it seems to perform decently. Besides, not huge difference can be sighted if it is compared to the upwind scheme in this case ( $Re=400$ ,  $129x129$  grid points). The errors between them have been calculated with the help of Norms.

*Table 1. Norms Upwind - Central Difference Scheme.  $Re=400$ , Grid  $129x129$  points*

	U	V
Norm 1	0.0136	0.0130
Norm 2	3.7758e-4	3.2749e-4
Norm Infinite	0.0559	0.0472

Table 1 reveals so little difference between each difference schemes, and both velocity components behave similarly in terms of errors. Norm 1 states the average error, which is complemented with the Root Mean Square error, that manifests that there errors are more punctual with biggest differences than not uniformly distributed along the curve. This particular trait is quite important to be mentioned. To finish up, Norm Infinite yields the maximum difference seen between both difference schemes which is minuscule.

Once achieved these satisfactory values -specially from Figure 6- it is concluded that the FORTRAN code is accurate enough to carry out the study of the cavity.

#### • Coarse Mesh Study

According to the operation conditions described in Problem characteristics, the cavity flow will be analyzed when it is operating with  $Re=65$ . The Coarse Mesh Study will be conducted with a  $10x10$  grid. The first stage will again be, to represent plots for U and V again for both discretization schemes for the convective term: upwind and central. First, in Figure 7, the U and V components for each scheme will be displayed along with the calculation of error norms. The

velocities will be evaluated in the same geometrical axis from Figure 2 to serve as a performance reference. Afterwards, a particularized post-processing study in each scheme will be done.

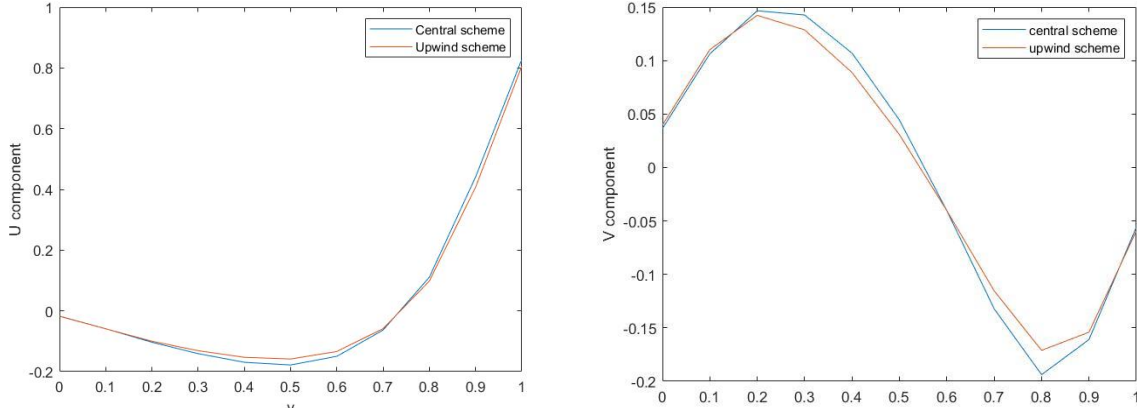


Figure 7. Coarse Mesh. U and V comparison for Upwind and Central schemes

Table 2. Norms Upwind - Central Difference Scheme. Re=65, Grid 10x10 points

	U	V
Norm 1	0.0091	0.0082
Norm 2	2.3017e-4	1.8402e-4
Norm Infinite	0.0536	0.0524

Both image and table of norms suggest that errors remain low even the case it is the coarse mesh. Interesting enough, if it is compared to the finer mesh but different Reynolds (Re=400) from the (Ghia, Ghia and Shin, 1982) case, it is seen these errors are even lower despite the fact that this mesh is 12.9 times coarser in each direction. Hence, a first interesting conclusion can be deduced: as Reynolds is increased, errors do so. If it is meditated thoroughly, it is rational: the N-S discretized terms are a model of the real viscous and convective terms, which are definitely non-linear and hard to numerically implement. Then, the higher values it gets, the more deviation will be seen in different schemes.

Now, both schemes will be analyzed using the post-processing ParaView software.

#### · Upwind Scheme

The theory fundamentals for the first-order upwind spatial scheme are supposed to be known but can be seen in (Ferziger and Peric, 2002) and (Versteeg and Malalasekera, 1995.). Nonetheless, serve the following explanation as a quick summary for this scheme.

The upwind discretization scheme possesses first order of accuracy – deduced from its Taylor series and applied to the linear advection problem- and satisfies the conditions of conservativeness, boundedness and transportiveness. It is known that the performance of this scheme is related to the grid refinement, as it may introduce a non-physical contribution due to false diffusion. However, this effect can be reduced as mesh is refined. Then, for the coarse mesh, some error coming from this false diffusion can be expected.

The upwind scheme determines the direction of the flow based on previous lectures or data. Hence, in our FORTRAN program, it is implemented with the following code:

$$\begin{aligned}
 aw(i, j) &= dw + \max(0.0, gw) \\
 ae(i, j) &= de + \max(0.0, -ge) \\
 as(i, j) &= ds + \max(0.0, gs) \\
 an(i, j) &= dn + \max(0.0, -gn) \\
 ap(i, j) &= dw+de+ds+dn+\max(0.0, -gw) + \max(0.0, ge) + \max(0.0, -gs)+\max(0.0, gn)
 \end{aligned}$$

Depending on the velocity vector coming from the previous iteration by the west-east and north-south pairs (gw,ge and gn,gs), it enforces the new velocity to move in the same direction.

Once loaded the results to ParaView and constructed a velocity field with the calculator imposing  $V=U^*i\text{Hat} + V^*j\text{Hat}$ , the following figures are interesting to be obtained.

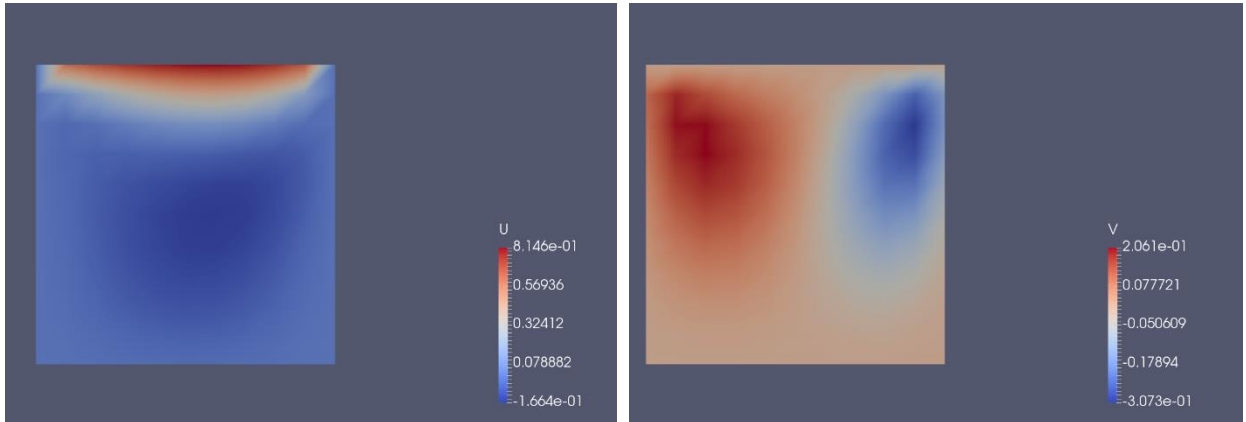
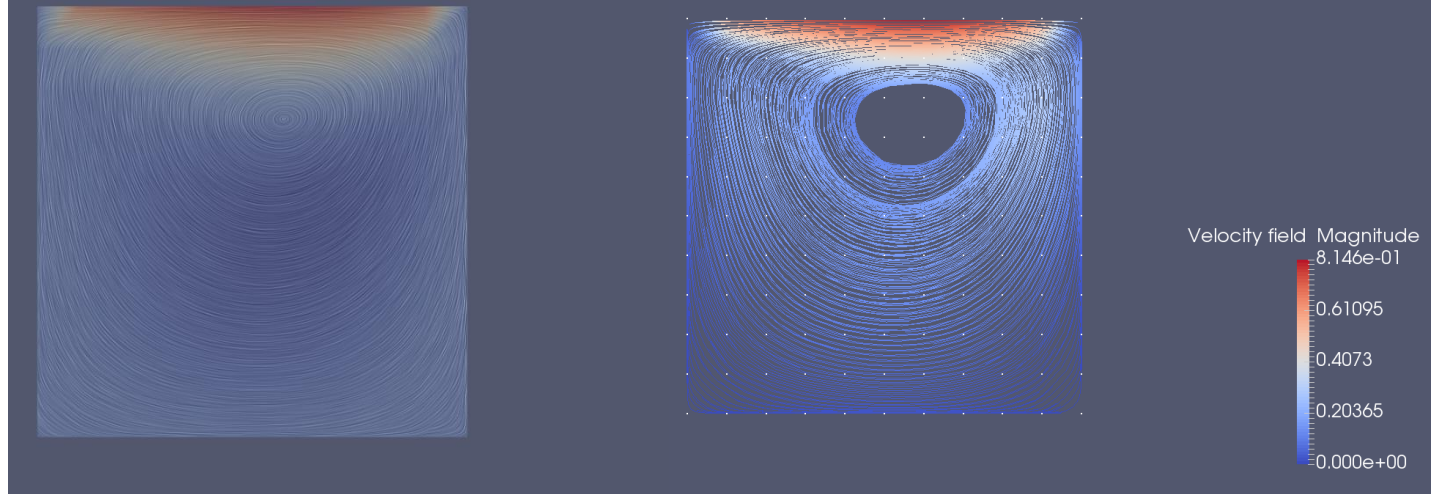


Figure 8. U and V components surface inside the cavity. Upwind scheme, Coarse Mesh

Figure 8. U and V components surface inside the cavity. Upwind scheme, Coarse Mesh reveals an approximate idea of both components, although it is clearly seen that refinement is necessary to be performed.

Besides, from (Ghia, Ghia and Shin, 1982) show two secondary recirculation zones in the bottom corners of the cavity. These recirculation zones have been greatly described and documented in

research papers as they appear in most cavities and backward-facing problems. Their behavior and shape depend on the geometric features of the “wall” but also on the fluid magnitudes. Any research paper would provide further information, yet (Rossiter, 1964) is recommended as it was one of the first to deal with them. Therefore, it is important to determine if this coarse mesh is able to capture both recirculation zones.



*Figure 9. Streamlines of Cavity's velocity field. Upwind scheme, Coarse mesh*

Streamlines for the velocity field have been computed with the ParaView software as Figure 9 displays: the first one with the “Surface LIC” filter and the second one with the “Streamline” filter applying one high precision line for each diagonal. It is clearly perceived that this scheme for this coarse mesh has not been able to capture the recirculation zones, although rough and general traits of the overall flow can be described as Figure 10 shows.

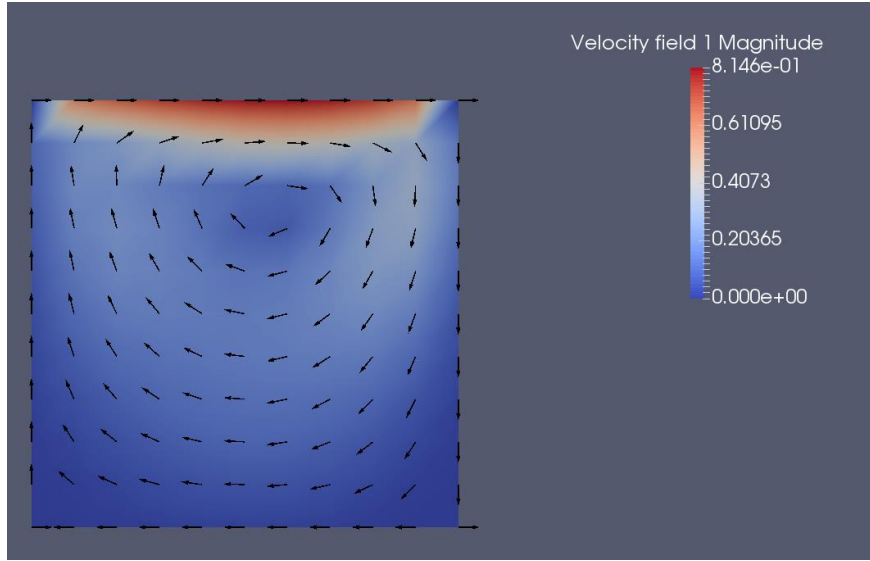


*Figure 10. Velocity field vectors*

#### . Central Scheme

The central scheme applied for a space derivative describes an average of the neighbour cell flux values to compute the current value of the magnitude. Due to this, a 2<sup>nd</sup> order of accuracy is obtained for a 1<sup>st</sup> order derivative as it is the convective term. However, if the linear advection problem is analyzed, it is seen that central schemes by their own may incur in instabilities of the result, although can be corrected with other non-central discretizations. The central scheme seems to introduce a slight oscillatory behavior depending on the problem faced and the operation conditions.

The central scheme also satisfies the principles of conservativeness, but boundedness, transportiveness and accuracy are only ensured for Peclet Number <2.

The implementation of the central scheme has been already explained in the section of: Problem characteristics.

Once transferred the results into the ParaView post-processing software, the following images of the velocity distribution can be obtained.

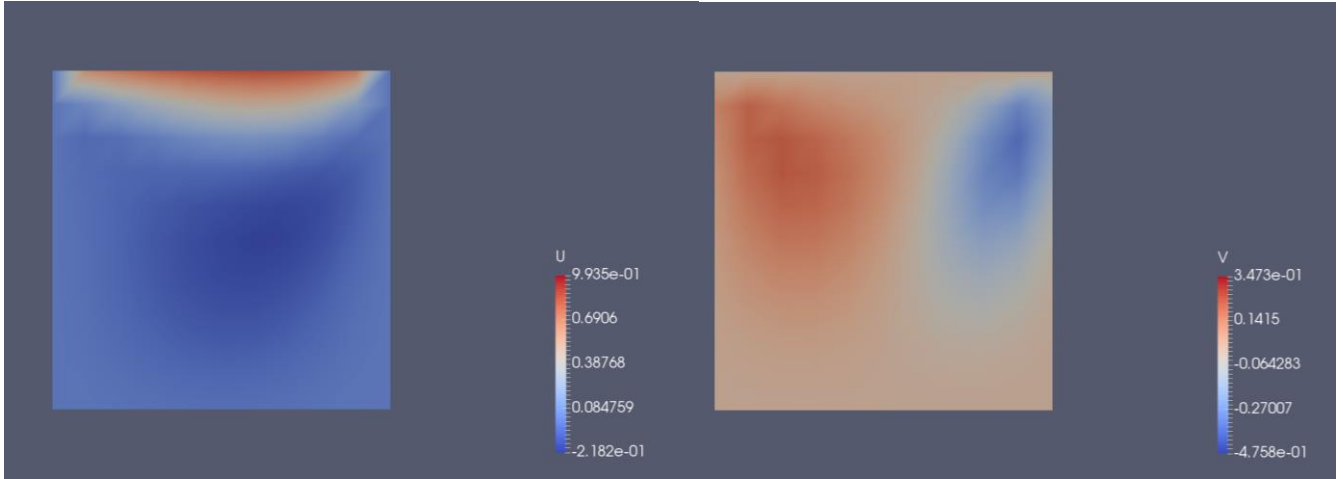


Figure 12.  $U$  and  $V$  components surface inside the cavity. Central scheme, Coarse Mesh

Figure 12 does not provide any different results from the ones obtained with the upwind schemes, except from the slight variation of magnitudes as they were already seen in Figure 7. Additionally, it is also recognized the need to compute a further refinement to this mesh. Then, recirculation zones should not be expected to be correctly captured when applying the same two both streamline functions that were applied in the upwind scheme. Figure 11 will show the results of this operation.

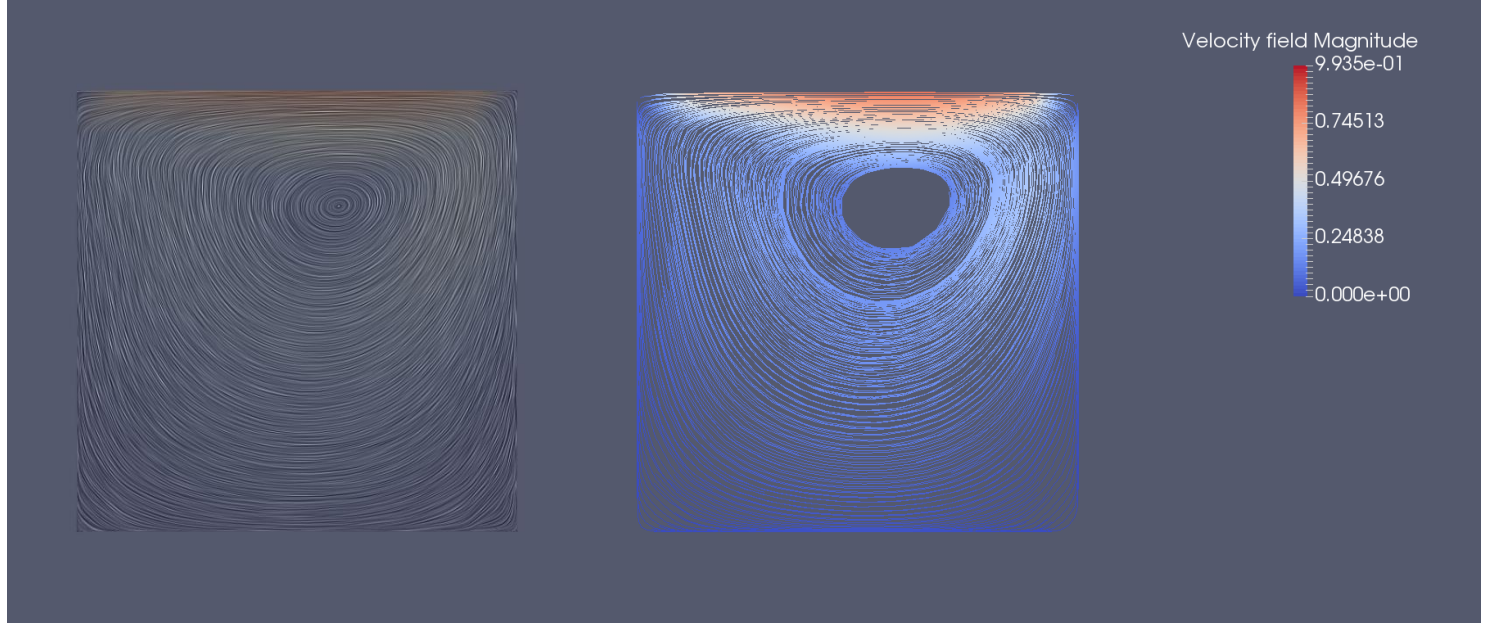


Figure 11 Streamlines of Cavity's velocity field. Central scheme, Coarse mesh

The recirculation zones that should appear in this case have not been correctly achieved. This endeavor is caused by the mesh insufficient resolution. Thus, a refinement of  $\times 25$  in each dimension will be applied.

### • Fine Mesh Study

The objective of a Fine Mesh is to be able to describe or obtain more detail of the fluid field inside the cavity but also minimize the error terms in all the fluid magnitudes. The fine mesh computed is an arbitrary 250x250 grid (25 times finer in each dimension than the coarser) which is supposed to release really accurate results -(Ghia, Ghia and Shin, 1982) obtained satisfactory results with 129x129 grid for higher Reynolds values-, which will be evaluated in the following lines. However, the computational cost has increased from few seconds (less than 10) to a little bit more than half a minute for the same computer (Cranfield library's PCs).

The results of the representation of both U and V components in the geometrical lines detailed in Figure 2 led to incredibly accurate terms as Figure 13 demonstrates. Both upwind and central difference schemes got overlapped even the central difference is one order superior in terms of accuracy in both components.

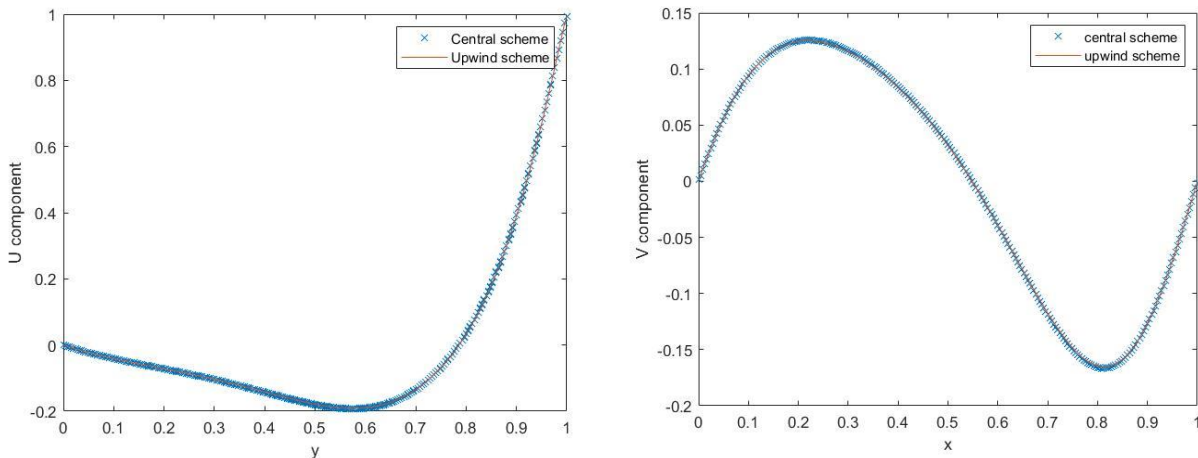


Figure 13. Fine Mesh. U and V comparison for Upwind and Central schemes

This fact is supported by the calculation of norms, which encompass tiny values as well.

Table 3. Norms Upwind - Central Difference Scheme.  $Re=65$ , Grid 250x250 points

	U	V
Norm 1	6.2104e-4	5.6884e-04
Norm 2	1.1357e-6	9.4748e-07
Norm Infinite	0.0041	0.0044

The upwind and central schemes show insignificant deviations from one another. The effect of the false diffusivity produced in the upwind scheme specially for coarse meshes could play an important role in this case, exaggerating the differences in the coarse mesh. Appropriately, as it is generally true but under certain constraints, the finer mesh, the most accurate solutions will be obtained. However, what is even more interesting in this case is the more detail obtained, as several physical phenomena may not be captured if mesh is not fine enough

Here, both Upwind and Central Schemes will be treated and evaluated jointly to be aware if a significant difference in the results take place.

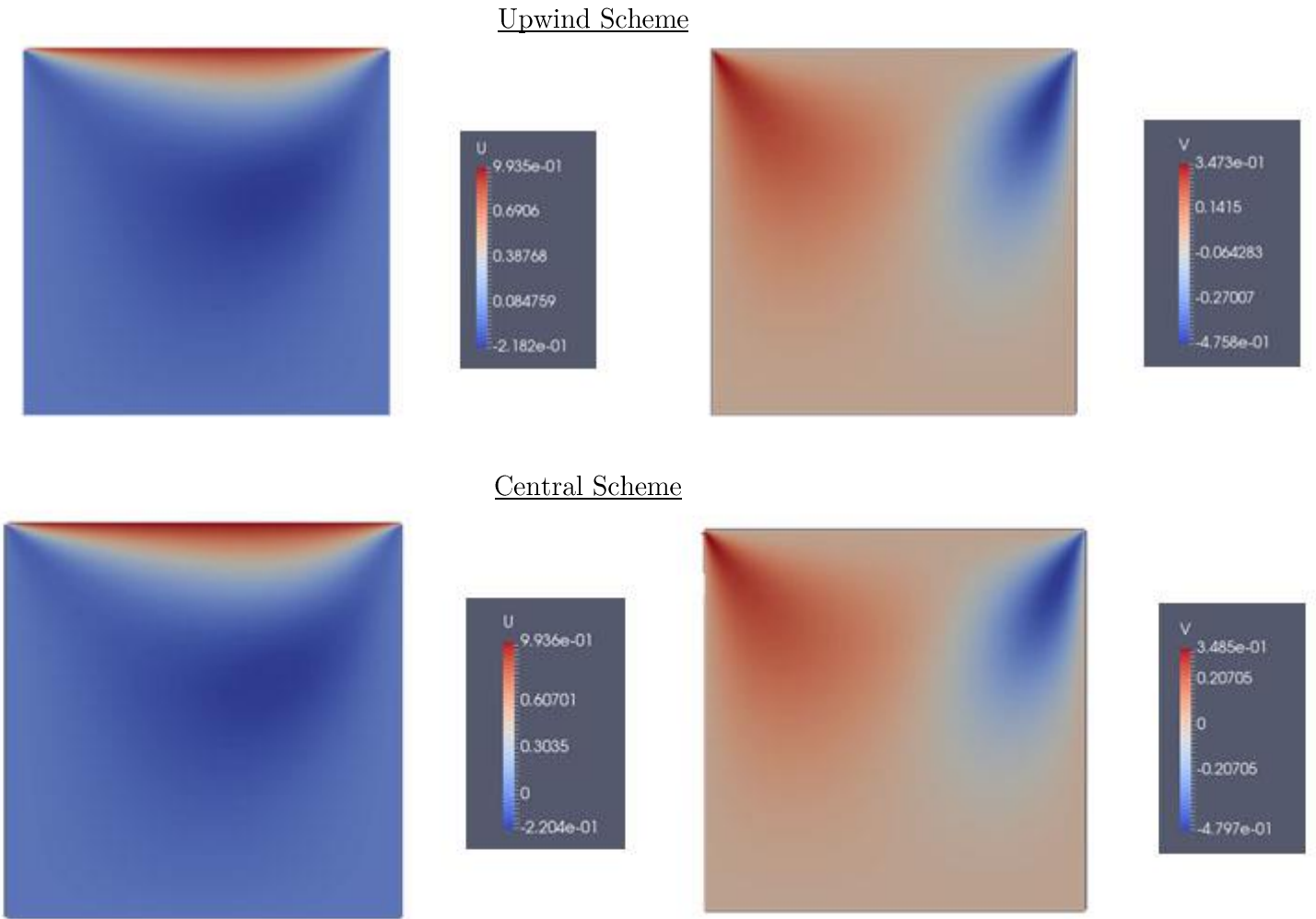


Figure 14.  $U$  and  $V$  components surface inside the cavity for both schemes (above: Upwind, below: Central). Fine Mesh

Figure 14 confirms the hypothesis that no significant difference would be seen in this case (Reynolds=65, Mesh:250x250). Both schemes look almost identical. Only slight differences can be noted in velocity maximum and minimum values. Due to the refinement, it seems that recirculation phenomena will be likely obtained once streamlines are computed.

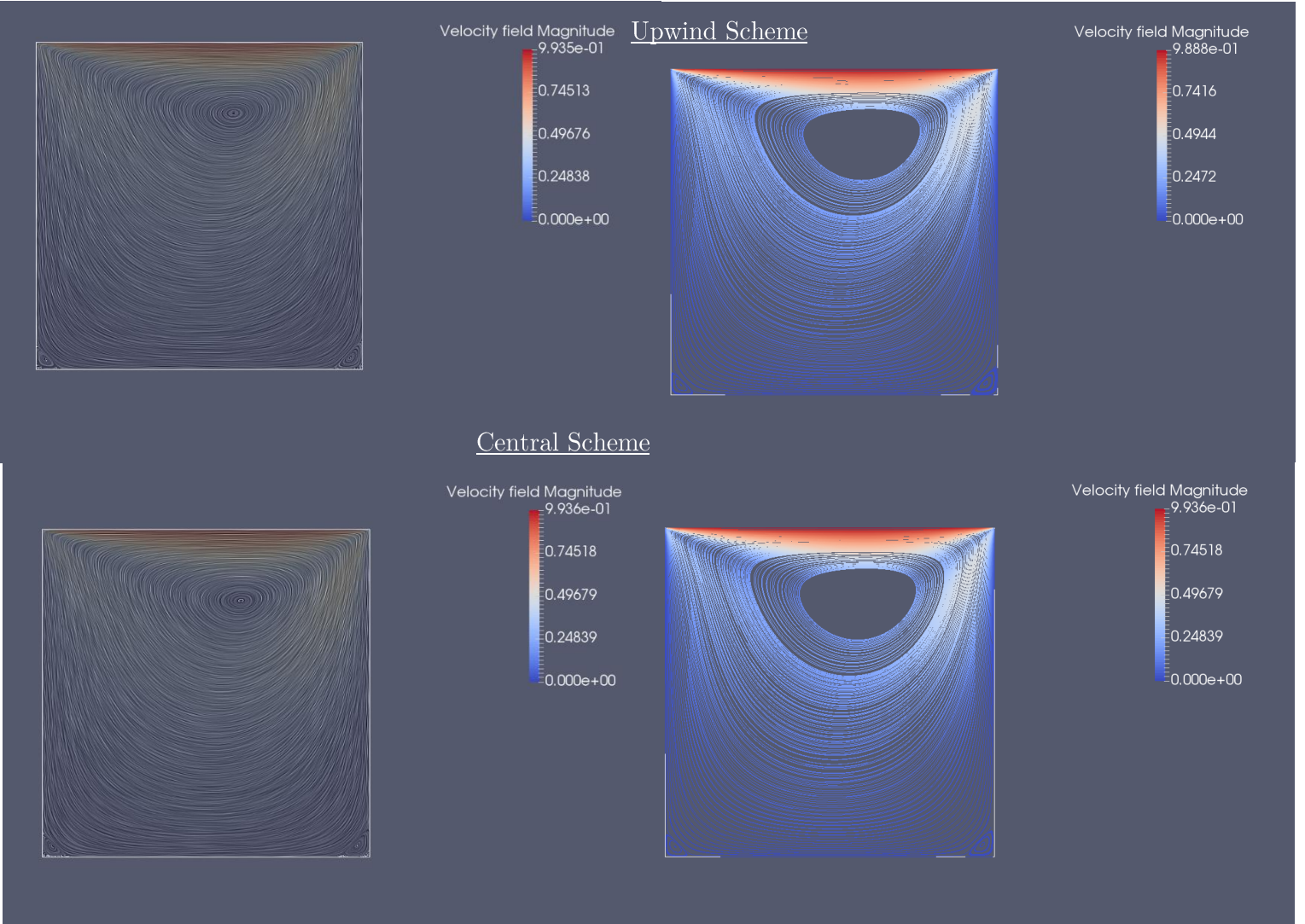


Figure 15. Streamlines of the velocity field for both schemes (above: Upwind, below: Central). Fine Mesh

Finally, the secondary recirculation zones in the bottom corners of the cavity for both schemes and by using two different streamlines tracer filters (Surface LIC and Streamlines) have been decently captured. Their rotation is obviously anti-clockwise and their velocity magnitude proximate to 0. According to (Ghia, Ghia and Shin, 1982), for  $Re= 1000$ , they obtained recirculation geometries of: 0.2 m height and 0.2 m wide for the left corner secondary recirculation and 0.4m height and 0.3 m wide for the right corner. Here, in the case of  $Re=65$  they are approximately 0.0913m height and 0.1247m for the left corner and 0.097 height and 0.1156 wide for the right corner. Firstly, this information is consistent in the manner that the right corner recirculation is bigger than the left and this difference will be increased as  $Re$  does so. Also, the effect of the Reynolds number will make their centers to approach in a really slow ratio to the center of the cavity. Others publications such as (Takemitsu, 1980) support and clarify this statement and even describe the phenomena of a -u flow over the cavity, obtaining a “specular”-

like result. The secondary recirculation will be logically bigger in the side the velocity vector from the upper free-stream condition points.

Additionally, it is thought to be interesting to compute the vorticity magnitude (Z direction) to confirm the adequate movement of the flow inside the cavity. It should be expected to have the highest values straight in the upper corners of the cavity, as flow from upper boundary condition faces directly those two edges and decomposing its primary unidirectionality into bidimensional flow.



*Figure 16. Vorticity Magnitude along the flow inside the cavity, Central Scheme, Fine Mesh*

Figure 16 demonstrates the accuracy of our hypotheses and explains the nature of the flow in both U, and V components of velocity seen and detailed in previous pages. Again, there's no apparent difference -even the limit values of vorticity are exactly the same- in both schemes, thence the only inclusion of the central's results. All these results confirm the idea that mesh is accurate, although for these first and second order of accuracy discretizations of the convective term may not be enough if Re is increased to much higher values.

## Conclusions

Firstly, the overall results -regarding particularly the fine mesh for both upwind and central difference schemes- show an outstanding performance of the numerical model applied: the pressure correction method. The graphs obtained with ParaView software and the plots of the velocity components in the mean geometric profiles of the cavity are consistent with the available bibliography and research papers. The most usual phenomena: stagnant flow point, recirculation zones, primary vortical sources, genera flow, etc have been greatly captured. Results seem to be really accurate and physical meaningful as well. Even the FORTRAN code has been proven to be well constructed since results for the Fine Mesh have been obtained within a minute whilst, from (Ghia, Ghia and Shin, 1982) their simulation for coarser meshes have been obtained after 16 minutes of computation. Nonetheless, there's no available information of their whole computer as it is known that computer specifications have a huge effect on computational time.

Besides, the Fine Mesh seems to be finer than meshes used for research such as (Ghia, Ghia and Shin, 1982), which worked decently with huge Reynolds numbers compared to the  $Re=65$  from this case. However, this refinement applied in our mesh could not be enough to describe flows for really high Reynolds as flow magnitudes in those cases are difficult to be modelled without introducing artificial (non-physical) components. Nevertheless, this fact could be overcome by using more accurate (higher order) schemes as (Rubin and Khosla, 1977), which withdrew satisfactory conclusions by applying 4<sup>th</sup> order methods to a grid of 17x17 points and  $Re=1000$ .

Regarding the Reynolds number, it has been clearly seen -particularly in Figure 6 and Figure 13- that the higher values it gets, the more errors and differences between schemes can be noticed. This information is not new at all, this fact is widely commented and explained at: (Nallasamy and Prasad, 1983.) Hence, from this type of simulations, we should be aware that the higher Reynolds flows to analyze, the more probability of obtaining non-accurate results and the more complex schemes must be developed to overcome this problem.

The present work leads to a wide variety of further steps to be carried out. The implementation of other convective schemes, the comparison with other numerical models, the analysis of the effect of the under relaxation parameter in each magnitude and to determine its best value, analysis of pressure behavior and the analysis of its oscillatory components, etcetera are just a few interesting ideas to complement the information displayed in this document. , I believe that the requirements and objectives of the assignment have been completed.

## References

- Ferziger, J.H. and Peric, M. (2002.) *Computational Methods for Fluid Dynamics*.
- Ghia, U., Ghia, K.N. and Shin, C.T. (1982) *High-Re Solutions for Incompressible Flow Using the Navier-Stokes Equations and a Multigrid Method\**.
- Golub, G.H. and van Loan, C.F. (1983) *Matrix Computations*.
- Landau L.D. and Lifshitz E.M. (1987) “Fluid Mechanichs,” *Institute of Physical Problems, USSR Academy of Sciences*, 6
- Nallasamy, M. and Prasad, K.K. (1983) *Note Spurious Solutions in Driven Cavity Calculations \**.
- Patankar, S. v and Spalding, D.B. (1972) *A CALCULATION PROCEDURE FOR HEAT, MASS AND MOMENTUM TRANSFER IN THREE-DIMENSIONAL PARABOLIC FLOWS*. Pergamon Press.
- Rossiter, J.E. (1964) “Wind Tunnel Experiments on the flow over rectangular cavities at subsonic and transonic speeds”
- Rubin, S.G. and Khosla, P.K. (1977) *Polynomial Interpolation Methods for Viscous Flow Calculations\**.
- Takemitsu, N. (1980) *On a Finite-Difference Approximation for the Steady-State Navier-Stokes Equations*.
- Turquand D'auzay, C. and Asproulis, N. (2013) *Pressure Correction TDMA (PC-TDMA) Incompressible Flow Solver Implementation*.
- Versteeg, H.K. and Malalasekera, W. (1995) *An Introduction to Computational Fluid Dynamics Second Edition*.

## Appendix 1: Medium Mesh Study

The grid of 40x40 will be studied as it is a requirement in the assignment but it will not describe further information than the presented in the coarse mesh (10x10, which was close to the grid of (Rubin and Khosla, 1977) which had 17x17 with higher order of accuracy discretization) neither the fine grid (250x250) whose results have been quickly obtained and represent the highest accuracy but also the higher chance to capture fluid phenomena. The operation conditions will remain the same,  $Re=65$ . Hence, this medium mesh is expected to entail an intermediate solution between the fine and coarse mesh analyzed in Results. Even more, it is possible that the spurious oscillation nature introduced by the central difference scheme can be finally sighted as it has not been seen in the previous cases.

Again, the U and V components will be plotted in the geometrical mean profiles of the lid driven cavity and a table of errors for the whole velocity field will be equally attached.

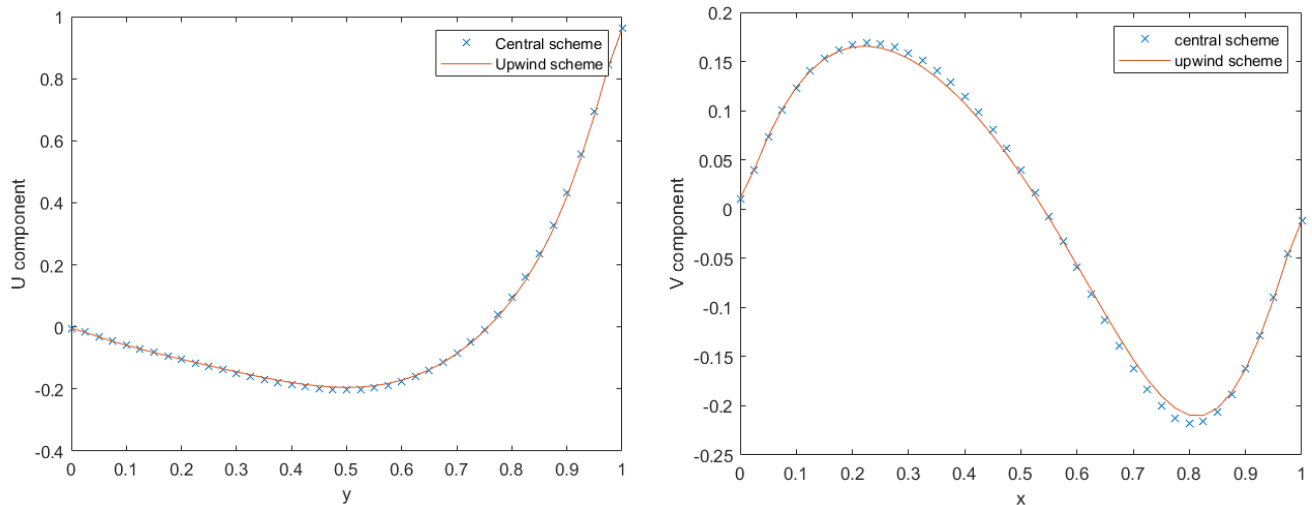


Figure 17. Medium Mesh Velocity comparison for both schemes in the geometrical medium profile

Table 4. Medium Mesh Deviations from both schemes for the velocity components

	U	V
Norm 1	0.0036	0.0033
Norm 2	3.5113e-5	3.0313e-5
Norm Infinite	0.0217	0.0229

The results deduced from the previous images strongly support the idea that this medium mesh will suppose an intermediate solution between · Coarse Mesh Study and · Fine Mesh Study.

However, is it also interesting to determine if the resolution (40x40 grid) is high enough to -for the 1<sup>st</sup> order of accuracy upwind scheme and 2<sup>nd</sup> order of accuracy central scheme- capture the recirculation zones seen in the fine mesh but that could not be obtained in the coarser. If the case is affirmative, for a bigger simulation, it would make a difference in terms of computational cost. The difference in this program is for about 10 seconds instead almost a minute for the fine mesh, which is not representative at all.

The streamlines have been obtained through applying the streamline filter to the upwind scheme and the Surface LIC filter to the central scheme. Results would not make a difference if the filters would be applied vice versa, yet the reason of applying different ones is to see that both filters perform correctly.

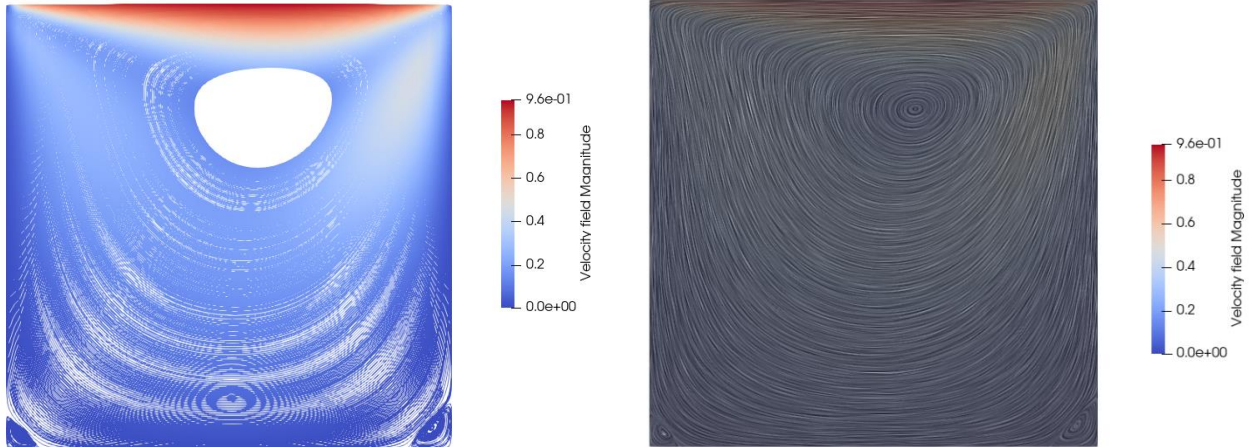


*Figure 18. Medium Mesh. Streamlines for: Upwind Scheme (left) and Central Scheme (right)*

Figure 18 demonstrates the accuracy of the 40x40 medium mesh to capture the same recirculation zones (with exactly the same dimensions) detected in the fine mesh and also present in most cases of literature for this benchmark problem. It is satisfactory, specially compared to (Ghia, Ghia and Shin, 1982), who needed a 129x129 (triple finer in each direction) mesh to capture the same phenomenon. However, this case has not been tested for higher Reynolds flows -up to 1000- where refinement is expected to be required as it has been explained in the Conclusions section.

Additionally, it seems stimulating to compute a fluid variable that has not been represented but could demonstrate the oscillatory behavior aimed in the central scheme, the pressure distribution with its norms of deviation for both schemes.

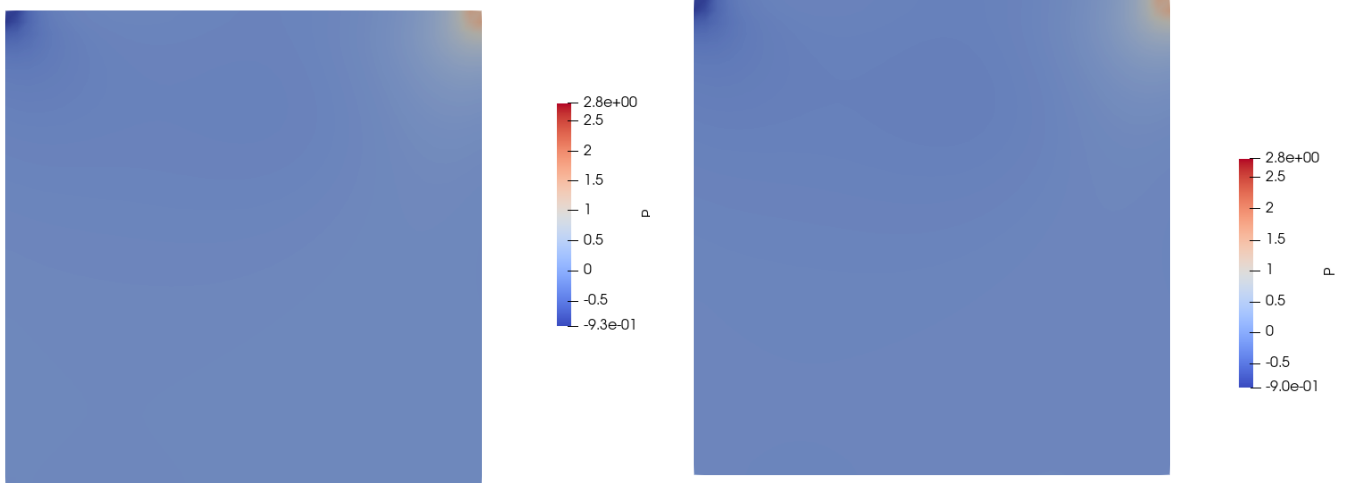


Figure 19. Medium Mesh. Pressure distribution: Upwind scheme (left) and Central Scheme (right)

Unfortunately, no oscillation in pressure can be detected as both graphs look almost identical. Besides, this deduction is backed up if norms of the deviation are computed in Table 5.

Table 5. Medium Mesh. Norms for the Pressure Deviation for both schemes

P	
Norm 1	0.0025
Norm 2	1.7923e-5
Norm Infinite	0.0069

To not be able to capture the oscillations for the pressure distribution, after reviewing the FORTRAN code several times, might be caused by the fact that  $Re=65$  is not high enough to display a strong difference between both schemes. As it was noticed in Figure 6, the higher the Reynolds number, the more difference between the upwind and the central difference schemes and also the finer mesh is required to physically describe the fluid phenomena that takes place.